EurJIC
European Journal of Inorganic Chemistry

Chemistry Europe
European Chemical Societies Publishing

Accepted Article

Title: Lattice dynamics and thermodynamic properties of bulk phases and monolayers of GaTe and InTe: a comparison from first-principles calculations

Authors: Andei Bandura, Alexey Kovalenko, Dmitrii Kuruch, and Robert Evarestov

To be cited as: *Eur. J. Inorg. Chem.* 10.1002/ejic.202000634

Link to VoR: https://doi.org/10.1002/ejic.202000634

WILEY-VCH

10.1002/ejic.202000634

Thermodynamics of In and Ga Monotellurides

Lattice Dynamics and Thermodynamic Properties of Bulk Phases and Monolayers of GaTe and InTe: a Comparison from First-Principles Calculations

Andrei V. Bandura[a], Alexey V. Kovalenko[a], Dmitry D. Kuruch[a], and Robert A. Evarestov*[a]

[a]Quantum Chemistry Department,
Institute of Chemistry, Saint Petersburg State University,
7/9 Universitetskaya Naberezhnaya, St. Petersburg, 199034, Russian Federation

*Correspondence to Robert A. Evarestov (E-mail: r.evarestov@spbu.ru)

Abstract
The hybrid density functional theory was used to study the structural, vibrational, and thermodynamic properties of stable and hypothetical bulk GaTe and InTe polymorphs, as well as their monolayer counterparts. Criteria based on the vibrational frequencies have been proposed to distinguish between different monolayer structures. Heat capacity, entropy, and Helmholtz free energy have been calculated by summing the vibrational contributions over the corresponding Brillouin zone. The relative stability of the considered systems has been estimated at different temperatures using the obtained Helmholtz free energy. Both the total energy and the Helmholtz free energy calculations confirmed that a free-standing monolayer originated from the monoclinic GaTe phase is less stable than its hexagonal analogs. It was also found that the temperature increase favors monolayer formation in the case of GaTe, but prevents it in the case of InTe.

1. Introduction

Gallium and indium tellurides are the layered crystals belonging to the family of group IIIA metal chalcogenides. Like the other compounds of this family, GaTe and InTe form the promising nanomaterials for photocatalysis, electronics, optoelectronics, and electrochemistry [1-5]. A lot of experimental and theoretical studies (see, for example, Refs [6-9]) have been done for other chalcogenides, namely, sulfides and selenides. Somewhat lower attention was paid to gallium and indium tellurides. The present theoretical study aims to compare the structural, electronic, vibrational, and thermodynamic properties of GaTe and InTe different bulk phases and their monolayers.

The structure of MTe (M = Ga, In) bulk crystals was investigated in dozens of experimental works. It was found [10-12] that the most stable phase of GaTe at ambient conditions has a monoclinic (*m*) structure (see Figure 1a) with space group (SG) 12, C2/*m*. Nevertheless, the metastable hexagonal 2H phase (see Figure 1b) with SG194 ($P6_3/mmc$) was also identified [13] in thin films using the electron diffraction technique. Authors [13] also reported that this polymorph transforms to the stable monoclinic structure upon heating. Much later, the existence of the hexagonal single crystals was confirmed [14]. Remarkably, both GaTe phases are composed of monolayers with the similar atomic arrangement (4-fold coordinated Ga and 3-fold coordinated Te), but exhibiting Ga–Ga chemical bonds of different orientations. One else rhombohedral layered modification, 3R (see Figure 1c) known [15] for gallium sulfide and found [16] to have almost the same energy as the 3R phase, might also be taken into account as a possible polytype of gallium telluride.

The crystal structure of the bulk InTe was investigated experimentally even more intensively than that of GaTe, but only the one stable low-pressure tetragonal (*t*) phase (see Figure 1d) with SG140 (I4/*mcm*) was reported [12,17]. Unlike GaTe, the InTe is not a layered crystal and consists of parallel $–InTe_2–$ and –In– chains. Nevertheless, there are several layered phases among the indium selenides. The low-pressure polymorphs of InSe exhibit the GaS-like (SG194) or GaSe-like (SG160) structure [18,19]. One of the high-pressure monoclinic (SG12) InSe polymorphs [20] also possesses the discernible layers (see Figure 1e), exhibiting the structure (designated here and below as *rβ*) which differs from the structure of layers in the monoclinic GaTe (designated as *rα,* see below). To distinguish two monoclinic phases we will label the SG of the high-pressure polymorph with the asterisk (*).

Both GaTe and InTe crystals demonstrate a semiconducting behavior having a band-gap of 1.5 - 1.7 [21-23] and 1.16 eV [23,24], accordingly. At elevated pressure, the monoclinic GaTe and tetragonal InTe undergo a phase transition to the face-centered cubic polymorphs, SG225, at approximately 10 and 5 GPa [25,26], respectively. This transition is followed by a tendency towards metallic behavior [12,25,26].

The variation of the lattice constants of stable GaTe and InTe phases with pressure and temperature has been investigated in several works. Thus, Schwarz et al. reported the value of 30 GPa for the bulk modulus of GaTe using the Murnaghan-type relation. Structural measurements of GaTe and InTe have also been made in the resent study [12] of Jacobsen et al. Particularly, third-order Birch–Murnaghan [27] equation of state has been used to obtain the bulk moduli of GaTe and InTe low-pressure phases, which turned out to be 36 and 29 GPa, accordingly. The linear thermal expansion coefficient of 1.7×10^{-5} K^{-1} has been measured in one [28] of the early works for monoclinic GaTe. The temperature dependence of the lattice parameters of tetragonal InTe was reported in Ref. [26] in the range from 297 to 505 K. As a result, the coefficient of linear thermal expansion was estimated at 2.0×10^{-5} K^{-1}. The pressure effect on the cell volume and interlayer spacing has also been investigated

within this phase's stability range. The fitting of volumetric data to the first order Birch equation provided the low-pressure InTe bulk modulus of 47 GPa [26].

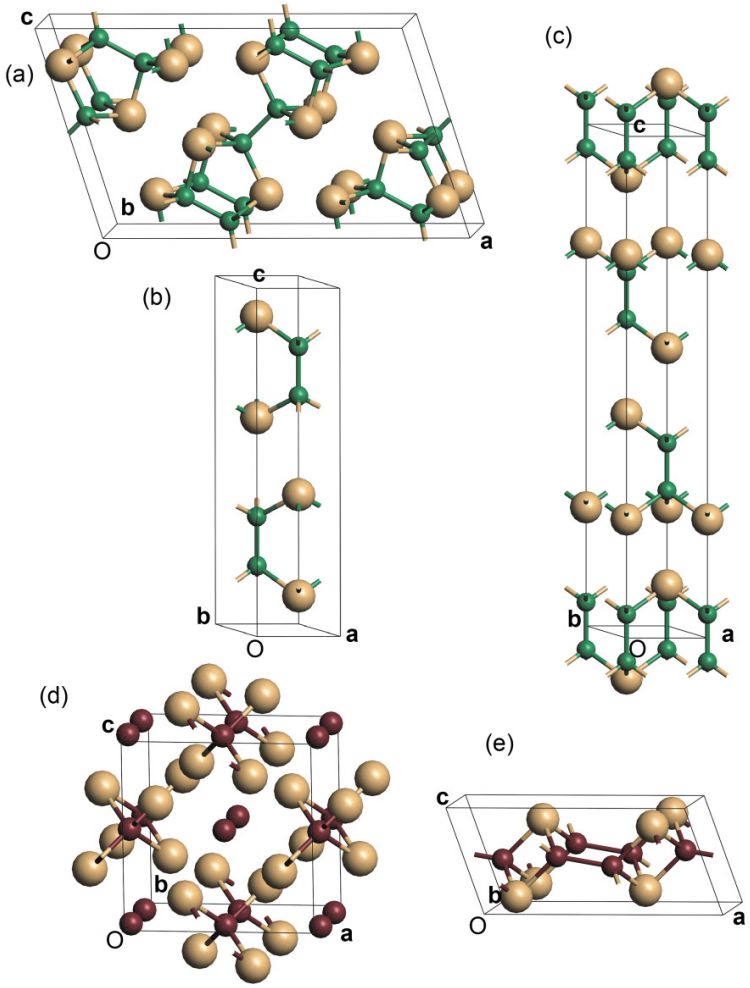

Figure 1. Conventional unit cells of five bulk phases considered in the present works. GaTe: monoclinic C2/*m* (a), hexagonal $P6_3/mmc$ (b), rhombohedral R-3*m* (c); InTe: tetragonal I4/*mcm* (d), and monoclinic C2/*m* (e). Legend: dark small spheres – metal atoms, large light spheres – Te atoms.

There are only a few experimental studies of the thermodynamic properties of bulk gallium and indium tellurides. Kerimov et al. were the first who measured the temperature dependence of the heat capacity of GaTe and InTe stable phases [29]. Later, Tyurin with coauthors [30,31] obtained the heat capacity of these substances in the temperature range from several K up to several hundred K. Based on these measurements, the heat capacity, entropy, enthalpy, and reduced Gibbs energy were calculated on the same temperatures. More recently, Back et al. have published [32] the dependence of specific heat on temperature for InTe.

Several experimental works have been devoted to the study of vibrational properties of stable gallium and indium tellurides. Most of them [33-38] consider the lattice vibrations of GaTe. Raman (R) active modes have been determined in Refs. [33,37,38], infrared (IR) reflection spectrum has been measured in Refs. [35,36], and both R and IR frequencies of GaTe were obtained in Refs. [34]. Authors of Ref. [38], besides the experimental measurements, perform the density functional theory (DFT) calculations intending to assign the experimental frequency values. The only known for us report on the InTe Raman spectrum was published by Nizametdinova [39].

No special publications could be found for the theoretical calculations of the structure and properties of GaTe and InTe bulk phases. In most of the published computational works the bulk phases are discussed with respect to the structure and properties of monolayers and thin multilayers. Due to the layer structure of most gallium chalcogenides and some of the indium chalcogenides, the possibility of forming two-periodic structures (monolayers, bilayers and so on) is a very urgent problem.

Few-layer GaTe flakes and thin films have been obtained experimentally since the late 90s [40], but have been studied most intensively in the past few years [41-46]. Many technics can be used for the synthesis of nano-sized objects. Among them can be mentioned the liquid or mechanical exfoliation of powder or single-crystal GaTe [41,42], chemical vapor deposition (CVD) [40], or physical vapor deposition (PVD) [45], and the molecular beam epitaxy [46]. It was found [13,40,42,45,46] that thin layers of GaTe exhibit the phase structure instability. Two factors are important in this matter: temperature and thickness. Generally, the initially acquired hexagonal thin films turn into monoclinic structures upon annealing at 500-700 °C, depending on their thickness. In this regard, the formation temperature may be the main factor for the phase control of GaTe films [45].

On the other hand, the authors of Ref. [46] have shown that the hexagonal (*h*) structure dominated when the thickness of just prepared sheets was less than a few tens of nm, while the monoclinic structure began to prevail for thicknesses greater than approximately 90 nm. In this sense, it was assumed [42] that there may be a critical thickness for the transition of the nanolayer from hexagonal to the monoclinic phase. In other words, the monolayers or multilayers composed of several hexagonal monolayers should be thermodynamically stable. In our work, we checked this statement for the free-standing monolayers.

As far as we know, no experimental evidence has been obtained for the existence of InTe nanolayers. Nevertheless, the InSe sheets with a few atomic layers' thicknesses can be synthesized [47]. On the other hand, many theoretical calculations have been made for monolayers and thin multilayers of both GaTe [41-43,48-50] and InTe [51-55]. Such properties as electron [41,48-53] and phonon [48,51,54] band structure have been considered in these works.

Taking into account the structure of existing layered low-pressure modifications of Ga and In bulk chalcogenides, three monolayer polymorphs whose symmetry is described by three different layer groups (LG), can be assumed (Figure 2a, b, c). The first two, *hα* and *hβ*, have the hexagonal 2D lattice with LG78 (p-6*m*2) and LG72 (p-3*m*1) and can be derived from the hexagonal [18] (2H, SG194) and rhombohedral [15] (3R, SG166) GaS model polytypes, correspondingly. The third one has the centered rectangular (*rα*) lattice, LG18 (c2/*m*11) originated from the monoclinic GaTe phase. The atomic disposition in the *rα* monolayer is more similar to that in the *hβ* monolayer than in the *hα* monolayer. In the *hα* structure the six chalcogen atoms are in a trigonal prismatic arrangement around the Ga–Ga bonded pair, whereas they are in the trigonal antiprismatic arrangement in *hβ* and *rα* structures. The main difference between *hβ* and *rα* layers is that all M–M chemical bonds are directed perpendicular to the *hβ* monolayer plane, while the M–M bonds roughly parallel to the layer plane also exist in the *rα* monolayer (see Figure 2c). The comparison between *hα*- and *rα*-GaTe monolayers' properties has been performed in several works [41,42,48]. First-principles calculations [41,48] of electronic properties of these monolayers have shown that both structures are intermediate-gap semiconductors with a similar band-gap. Moreover, the *hα*-monolayer is an indirect band-gap semiconductor, while the *rα*-monolayer reveals a direct band-gap. As expected, when the thickness of the nanolayer increases, the band-gap decreases approaching the bulk value [41,50]. Shangguan et al. [48] calculated the vibrational properties

of *hα*- and *rα*-monolayers and confirmed their dynamical stability.

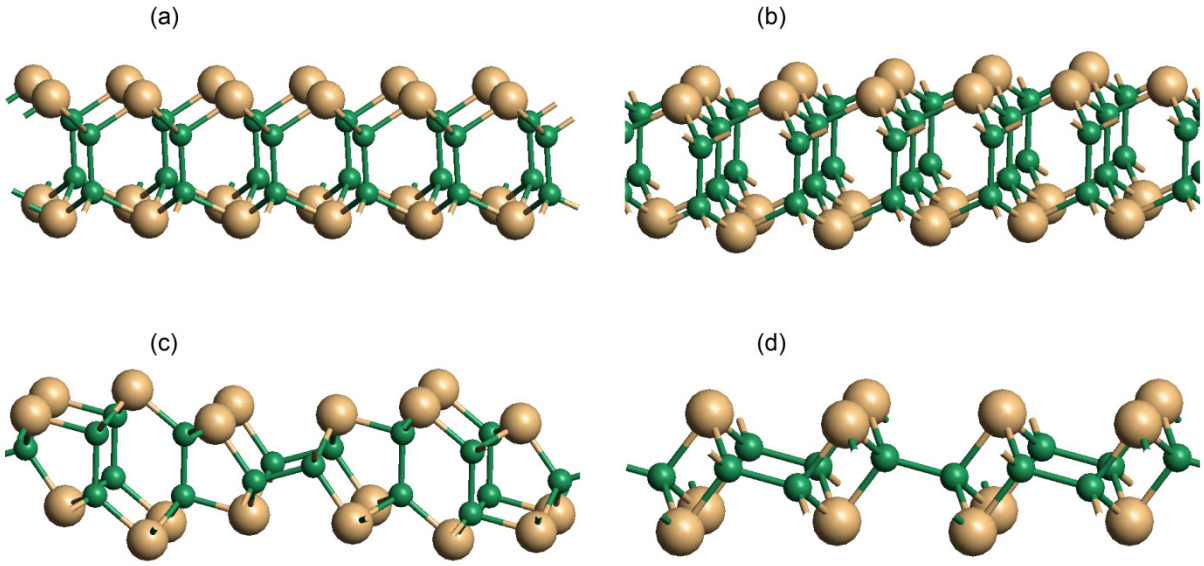

Figure 2. Optimized structure of *hα* (a), *hβ* (b), *rα* (c), and *rβ* (d) monolayers. Legend: dark small spheres – metal atoms, large light spheres – chalcogen atoms.

The hexagonal GaTe *hα* structure exhibits superior thermoelectric characteristics because of lower thermal and higher electrical conductivities [48]. Thermoelectric materials, which enable direct energy conversion between heat and electricity, have attracted considerable attention for clean power generation [56-58]. Gallium chalcogenides not only demonstrate thermoelectric properties themselves [21,32,48,53], but can also be used as dopants to improve thermoelectrics of other compounds, such as SnTe [57].

Zólyomi et al. [51] explicitly compared the stability of *hα* and *hβ* InTe monolayers polymorphs. They have also compared these monolayers' electron and phonon properties and found a close similarity between them. Recently, the same layers have been studied by Touski el al. [55]. A comparison between structural and electronic properties of *hα* and *hβ* monolayers and bilayers was also performed for vairous indium and gallium chalcogenides in Ref. [59]. The explicit comparison of *rα* and *rβ* monolayers originated in different monoclinic phases has never been performed. As can be seen in Figure 2c, d, *rβ* layers, unlike *rα* layers, have only the M–M bonds, which are approximately parallel to the plane of the layer.

In this work, we present a first-principles study of gallium and indium tellurides' structure and stability. The results of phonon calculations are used to compute the heat capacity, entropy, and Helmholtz free energy of several bulk phases and monolayers. As far as we know, the thermodynamic properties of GaTe and InTe compounds have not been theoretically investigated before. However, knowledge of the free energy is necessary to estimate the temperature-dependent stability of the possible new types of GaTe and InTe bulk phases and monolayers, as well as to obtain useful information for their suggested synthesis. The transition from bulk crystals to nanoobjects (monolayers, nanoribbons, and nanotubes) makes it possible to offer new promising applications of gallium and indium chalcogenide systems. The monolayers considered in this work are the probable precursors of the single-walled and multi-walled nanotubes, which are currently almost unstudied. In this regard, one of the long-term goals of our study is to select the most thermodynamically stable monolayers for the possible nanotube construction.

This article is organized as follows. In the Computational details section, we consider the methods and models used in this study. In the next section, we present and discuss the results obtained for the structural, vibrational, and thermodynamic properties of bulk and monolayer GaTe and InTe systems. The main results of our study are presented in the Conclusion section.

2. Computational details

Our first-principles computations have been accomplished with the periodic DFT using the two types of hybrid exchange-correlation functionals. The first one is the modified PBE0 functional [60], containing 13% of the Hartree-Fock exchange. As was shown by Kuzmin et al. [61], 13% of the Hartree-Fock exchange provides a good reproducibility of the structural, electronic, and phonon characteristics of solid metal oxides. This has been confirmed by our previous calculations [16] of layered gallium sulfides and selenides. However, preliminary calculations of bulk indium tellurides have shown that both the original PBE0-25% and PBE0-13% give the incorrect stability sequence of InTe solid phases. Moreover, both methods gave imaginary frequencies at the Γ point of the Brillouin zone (BZ) for the tetragonal InTe phase, which should be stable according to all experimental measurements [17]. For this reason, the vibrational and thermodynamic properties of GaTe and InTe, indicated below, were calculated using the M06 hybrid exchange-correlation functional recommended for applications involving main-group thermochemistry and noncovalent interactions [62]. As shown in the next section, the PBE0-13% and M06 functionals can almost equally well reproduce the stability and electronic properties of the known GaTe phases. However, the M06 functional can reproduce the correct stability of the observed tetragonal InTe phase, although it somewhat overestimates the lattice constants. Nevertheless, the phonon frequencies obtained by PBE0-13% and by M06 are very close for the values greater than 30 cm^{-1}.

The basis set of atomic orbitals has been used to expand the electron Bloch functions as it is implemented in CRYSTAL17 computer code [63,64]. In contrast to a widely-used plane-wave basis, the localized atomic basis allows avoiding the artificial introduction of 3D periodicity for 2D layered systems. The all-electron basis pob_DZVP_rev2 [65] has been applied for Ga, and m-pVDZ-PP_Heyd [66] basis and corresponding effective core pseudopotentials have been applied for In and Te atoms. The subvalence 4*s*- 4*p*-, and 4*d*-shells have been explicitly included for In and Te atoms. In calculating the direct lattice sums of one-electron and two-electron Coulomb and exchange integrals, an enhanced threshold set [64] 10^{-8}, 10^{-8}, 10^{-8}, 10^{-9}, and 10^{-18} has been used.

The Brillouin zone of InTe and GaTe bulk crystal of SG 194 has been sampled using Monkhorst-Pack [67] 16×16×4 **k**-point mesh. In other cases, the mesh in the reciprocal space was set inversely proportional to the corresponding cell constants to ensure approximately the same density in the **k**-point sampling grid.

To consider the van der Waals dispersion contribution to the interactions between InTe and GaTe layers, we have applied the DFT-D3 zero-damping approach [68] available in the CRYSTAL17 code. Within this approach, the D3 dispersion correction (DC) includes a damped atom-atom pairwise empirical term added to the Kohn-Sham - DFT total energies. The default CRYSTAL17 [64] built-in values were exploited for DC parameters.

All the considered structures have been optimized. The tight optimization criteria of 10^{-5} a.u. for the average gradient and 3×10^{-5} a.u. for the mean displacement have been implemented to calculate the phonons. Bulk moduli have been computed using the third-order Birch–Murnaghan [27] equation via the built-in CRYSTAL17 procedure [69]. A direct

(finite-displacement) approach [70,71] was applied to calculate the phonon frequencies and dispersion curves. For this purpose, the supercells containing up to 16 and 36 primitive unit cells have been created for bulk and layer systems, respectively. Additionally, the CRYSTAL17 interpolation technique [64] was used to double or quadruple the number of **k**-points using the INTERPHESS keyword.

3. Results and discussion

3.1. Structural and electronic properties of bulk and monolayer GaTe and InTe

Most of the considered bulk phases are composed of monolayers, weakly interacting via the van der Waals forces. To investigate the relative stability of different bulk phases and their monolayers, we have considered the same set of structures based on the experimentally observed modifications of bulk GaTe and InTe. In this set, we included the monoclinic (SG12), hexagonal 2H (SG194), and tetragonal (SG140) structures. The first two structures correspond to the stable phases of gallium telluride, while the last one is a stable modification of the indium telluride. Two extra hypothetical polymorphs were also added to the regarded series, namely the 3R polytype (SG166), experimentally detected for GaS [15], and the high-pressure modification with InSe monoclinic structure [20] (SG12).This choice is explained, on the one hand, by the real existence of the phases under consideration, and, on the other hand, by the presence of the main types of monolayers inherent in gallium and indium chalcogenides. In particular, the four monolayer modifications have been discussed in the Introduction section, *hα*, *hβ*, and *rα, rβ*, which correspond to hexagonal and monoclinic bulk phases, accordingly.

Table 1. Calculated and experimental[a] properties of known bulk GaTe and InTe phases.

Compaund, Space group	Method	*a*, Å	*b*, Å	*c*, Å	β°	E_{form}[b], kJ mol^{-1}	*B*[c], GPa	E_{gap}[d], eV
GaTe	PBE0-13%	17.60	4.100	10.55	105.4	0.00	20	1.8
C2/*m*	M06	17.92	4.110	10.69	106.3	0.00	26	2.3
	experiment	17.404 (2) [10]	4.077 (2) [10]	10.456 (2) [10]	104.44 (1) [10]	-	36.1 (4) [12]	1.7 [23]
GaTe	PBE0-13%	4.082	-	16.93	-	1.94	25	1.0
$P6_3/mmc$	M06	4.084	-	17.36	-	1.90	28	1.6
	experiment	4.060 [13]	-	16.96 [13]	-	-	-	1.5 [40]
InTe	PBE0-13%	8.671	-	7.271	-	0.00	22	0.6
I4/*mcm*	M06	8.822	-	7.277	-	0.00	21	1.2
	experiment	8.454 (2) [17]	-	7.152 (6) [17]	-	-	28.7 (5) [12] 46.5 (5) [26]	1.2 [23]

[a] The uncertainty on the last digit is indicated in parentheses, if available.
[b] The total electronic energy with respect to the experimentally most stable phases, *C*2/*m* (SG12) for GaTe and I4/*mcm* (SG140) for InTe.
[c] Bulk modulus.
[d] Band gap.

In Table 1, we compare the lattice constants, relative total energies, bulk moduli, and band gaps obtained using PBE0-13% and M06 functionals with the available experimental data for the experimentally proven bulk phases. In Table 2, we report the same properties calculated for the hypothetical rhombohedral 3R, monoclinic (of InSe high-pressure type),

and tetragonal phases of GaTe and hypothetical monoclinic, hexagonal (2H), and rhombohedral (3R) phases of InTe.

Data of Table 1 indicate that PBE0-13% accurately reproduces the experimental cell constants of the crystals considered. The mean deviation of calculated values from the experimental data is about 1%, though, for the InTe tetragonal phase, the deviations are greater than 2%. The M06 functional provides the deviations, which are, on average, two times greater. The band gaps are reproduced by both functionals with approximately equal quality, although PBE0-13% mostly underestimates them, while M06 – overestimates. Bulk moduli calculated by the third-order Birch–Murnaghan [27] equation are somewhat lower than the experimental values, but are reasonable.

In Tables 1 and 2, we give the formation energies of polymorph estimated via the relation:

$$E_{\text{form}}(X) = E_X/n_X - E_0/n_0, \quad (1)$$

where E_X is the total energy of polymorph X per unit cell (UC), E_0 is the similar total energy of the conventional most stable polymorph of the same composition, n_X and n_0 are the corresponding numbers of formula units. The computed total energy difference, between the hypothetical polymorphs and the most stable phases allows us to estimate the principal possibility of their real existence. For example, the difference between the total energies of 3R (SG166) and monoclinic modifications (corresponding to the ground state) of GaTe is less than 2 kJ mol^{-1} and very close to that of E_{form} for the 2H phase (which is metastable but does exist [13]). The value of E_{form}(3R) obtained by M06 functional is even lower than the value of E_{form}(2H). Thus, we can tentatively conclude that 3R polytype based on *hβ*-layers may be found experimentally. A more definite conclusion can be made after analyzing the free energy difference given in section 3.3. In contrast to the 3R polytype, two other considered GaTe phases (tetragonal and high-pressure monoclinic) have the formation energies greater than 10 kJ mol^{-1}, and should not be regarded as really possible at ambient conditions.

Table 2. Calculated properties of hypothetical bulk GaTe and InTe phases.

Com-paund	SG	Method	*a*, Å	*b*, Å	*c*, Å	β°	E_{form}[a], kJ mol^{-1}	B[b], GPa	E_{gap}[c], eV
GaTe	I4/*mcm*	PBE0-13%	8.404	-	6.786	-	29.7	26	0.7
		M06	8.505	-	6.836	-	23.5	29	1.4
	R-3*m*	PBE0-13%	4.099	-	25.22	-	1.97	25	0.9
		M06	4.104	-	25.87	-	1.60	28	1.6
	C2/*m**[d]	PBE0-13%	10.31	4.090	6.253	103.5	16.5	7	0.6
		M06	10.58	4.091	6.126	104.5	15.0	15	1.1
InTe	$P6_3/mmc$	PBE0-13%	4.327	-	17.72	-	-1.51	23	0.8
		M06	4.323	-	18.33	-	2.89	25	1.4
	R-3*m*	PBE0-13%	4.340	-	26.44	-	-1.38	24	0.7
		M06	4.332	-	27.39	-	3.23	25	1.5
	C2/*m*[e]	PBE0-13%	17.98	4.375	10.92	100.9	-1.40	18	1.2
		M06	18.81	4.338	11.17	103.5	2.77	23	1.8
	C2/*m**[d]	PBE0-13%	12.17	4.419	5.084	109.2	-0.09	18	0.6
		M06	12.13	4.390	5.629	108.5	8.13	16	1.1

[a] The total electronic energy with respect to the experimentally most stable phases, *C*2/*m* (SG12) for GaTe and I4/*mcm* (SG140) for InTe.
[b] Bulk modulus.
[c] Band gap.
[d] Monoclinic phase of high-pressure InSe-structure.
[e] Monoclinic phase of GaTe-structure.

The formation energies of hypothetical InTe phases presented in Table 2 demonstrate a more complex relative order than that considered above for the GaTe phases. All the values of E_{form} obtained using PBE0-13% functional are small and negative, which seems unrealistic. This fact was one of the reasons that made us use another DFT functional. Exchange-correlation functional M06, unlike PBE0-13%, correctly reflects the experimental fact that the tetragonal phase is the most stable InTe polymorph. Thus, we can assume that the M06 results for InTe compounds are more reliable than the PBE0-13% results. The values of E_{form} calculated using M06 for all phases in Table 2 (except the high-pressure monoclinic polymorph) are around 3 kJ mol^{-1}, which are quite small and suggest that some of them may be discovered someday experimentally. In contrast, the C2/*m** phase ($E_{\text{form}}^{\text{M06}} = 8.1$), originated from the high-pressure InSe modification, can hardly be found under ordinary conditions.

Table 3. Calculated properties of GaTe and InTe monolayers. The angle γ equals 120° in hexagonal (*h*) layers and 90° in centered rectangular (*r*) polymorphs.

Com-paund	SG	Label	Method	*a*, Å	*b*, Å	E_{form} [a], kJ mol^{-1}	ΔE [b]	E_{gap} [c], eV
GaTe	p-6*m*2	*hα*	PBE0-13%	4.081	-	8.7	0.0	2.4
			M06	4.073	-	13.4	0.0	2.9
	p-3*m*1	*hβ*	PBE0-13%	4.097	-	9.3	0.6	2.3
			M06	4.092		13.5	0.1	2.8
	c2/*m*11 [d]	*rα*	PBE0-13%	4.085	23.51	12.5	1.9	2.3
			M06	4.089	23.55	15.7	2.3	2.8
	c2/*m*11* [e]	*rβ*	PBE0-13%	4.076	10.015	31.7	21.0	1.9
			M06	4.054	9.966	35.2	21.8	2.4
InTe	p-6*m*2	*hα*	PBE0-13%	4.320	-	13.1	0.0	2.2
			M06	4.310	-	19.7	0.0	2.7
	p-3*m*1	*hβ*	PBE0-13%	4.333	-	13.4	0.4	2.1
			M06	4.318	-	20.3	0.6	2.7
	c2/*m*11 [d]	*rα*	PBE0-13%	4.349	25.21	14.6	1.7	2.1
			M06	4.313	25.33	22.3	2.7	2.5
	c2/*m*11* [e]	*rβ*	PBE0-13%	4.317	11.23	30.27	17.19	1.9
			M06	4.287	11.41	40.51	20.86	2.4

[a] The total electronic energy with respect to the experimentally most stable phases, C2/*m* (SG12) for GaTe and I4/*mcm* (SG140) for InTe.
[b] Relative monolayer energy.
[c] Band gap.
[d] Monolayer from monoclinic GaTe-structure.
[e] Monolayer from monoclinic high-pressure InSe-structure.

Hexagonal monolayers *hα* and *hβ* (Figure 2a, b), as well as the rectangular *rβ* monolayer (Figure 2d), are cleaved from 2H, 3R, and C2/*m** bulks parallel to a crystallographic plane (0 0 1). The rectangular *rα* (Figure 2c) is cleaved from the monoclinic phase parallel to the plane (-2 0 1). The lengths of M–Te and M–M chemical bonds in monolayers are rather conservative, as shown in Figure S1 of Supporting Information. Table 3 demonstrates the properties calculated for monolayers extracted from hexagonal, rhombohedral, and two monoclinic layer polymorphs of MTe (M = Ga, Te). The difference between the formation energy of this and the most stable *hα* monolayer, Δ*E*, is indicated in

the column next to the E_{form} column. Taking into account the results provided by both DFT functionals, the stability (at temperature $T = 0$) of those monolayers can be sequenced in the following order: $h\alpha \geq h\beta > r\alpha >> r\beta$. The total energy of $h\beta$ monolayer is greater than that of $h\beta$ monolayer by less than 0.6 kJ mol^{-1}, verifying that $h\alpha$ and $h\beta$ hexagonal structures are almost equal on energy as it takes place for the bulk phases. The most important conclusion from the data in Table 3 is that rectangular monolayer is less stable than the hexagonal monolayers, although the difference between total energies ΔE is not large and amounts to 2-3 kJ mol^{-1}. Thus, our data confirm the conclusions of the experimental analysis [42,46] about the strong dependence of the phase state of GaTe nanolayers on the number of monolayers of which they are composed. We can also conclude from our results that the formation of the hexagonal monolayers from the observed InTe tetragonal phase requires more energy (by 7 kJ mol^{-1}) than the formation of monolayers of the same structure from the GaTe monoclinic phase. Finally, the calculated values of ΔE, listed in the seventh column of Table 6, show the extremely high relative energies of rectangular monolayer $r\beta$ extracted from the monoclinic high-pressure InSe-structure. Because of that such a monolayer was excluded from further analysis.

In section 3.3, we present the thermodynamic analysis of the relative stability and its temperature dependence for the bulk and monolayer structures selected using the total energy calculations described above.

3.2. Phonon frequencies for bulks and monolayers of GaTe and InTe

To compare the vibrational properties of the bulk phases and monolayers considered in the previous section we have calculated the phonon frequencies at different **k**-points of the corresponding 3D or 2D BZ. Dynamical stability of the indicated in Tables 4 – 8 bulk and monolayer structures are confirmed by phonon dispersion calculations described at the end of this section.

In Tables 4 – 8 we present the results obtained for zone-center vibrational modes. As was stated in the Introduction section, there are several experimental studies [33-38] of the vibrational spectra of a GaTe monoclinic crystal. It should be noted that in most experimental works the frequencies for Raman scattering spectra have been measured. We have found only two early works [35,36] where the frequencies of infrared reflection spectra of GaTe were reported and assigned to symmetry group irreducible representations (Irreps). The purpose of Table 4 is to compare our results obtained for the bulk phase with those of the 5 selected experimental works. It can be seen in Table 4 that calculated Raman frequencies are in satisfactory agreement with the experimental values reported. Accordance with the IR experimental frequencies is rather worse. This discrepancy may partially be explained by experimental errors that can be expected, taking into account the discrepancies between the IR values measured by different authors.

The last column of Table 4 lists the frequencies calculated for corresponding $r\alpha$ monolayer. It is important to note that neither the dynamical representations nor the IR or R activity change when the monolayer is isolated. Indeed, the primitive UC of the monoclinic (m) phase comprises one UC of the monolayer, and both the SG of bulk and LG of monolayer have the same isogonal point group (C_{2h}). The composition of optical modes is as follows:

$$\text{R: } 12A_g + 6B_g; \quad \text{IR: } 5A_u + 10B_u \quad (m\text{-bulk and } r\alpha\text{-monolayer}), \tag{2}$$

Interestingly, no silent (S) modes were found in this system. The average deviation of monolayer frequencies from bulk values is about 2 cm^{-1}.

Table 4. Calculated and experimental phonon frequencies (cm^{-1}) in monoclinic bulk phase of GaTe and calculated frequencies in corresponding monolayer.

N		*m*-Bulk				*rα*-Monolayer
	R modes	This work	[33]	[34]	[37]	This work
1	A_g	40	41	41	41	40
2	B_g	42				41
3	A_g	53	53	52	53	53
4	B_g	54	57	58	57	55
5	B_g	62				61
6	A_g	66	67	67	67	64
7	A_g	78	76	76	77	72
8	A_g	114	110	110	111	109
9	A_g	120	115	115	116	115
10	A_g	156	153	155	155	156
11	B_g	167	163	164	167	167
12	B_g	171	169	170	172	172
13	B_g	178			179	178
14	A_g	185	177	178	181	182
15	A_g	216	210	208	212	218
16	A_g	218			271	221
17	A_g	288	271	271	272	291
18	A_g	301	284	284	288	304
	IR modes	This work	[35]	[34]	[36]	This work
1	B_u	44			49	45
2	A_u	50			94	51
3	A_u	67			118	67
4	B_u	91		90	89	86
5	B_u	94			97	93
6	B_u	116		116	112	110
7	B_u	143	130	145	124	141
8	B_u	165	141	163	141	166
9	A_u	169			131	170
10	A_u	174	139	(169,174) [b]	143	175
11	A_u (TO) [a]	178	174	(185) [b]	174	179
	A_u (LO) [a]	204	199		199	–
12	B_u	200	158	180	157	203
13	B_u	213	195	200	193	216
14	B_u	223		217	212	222
15	B_u	290		271	266	292

[a] Only one mode was found to exhibit a noticeable LO-TO splitting.
[b] Frequencies were not assigned to vibrational modes.

As mentioned above, for comparison purpose, we also considered the hypothetic monoclinic phase of InTe, for which there are no experimental data. The comparison of bulk and monolayer frequencies of monoclinic InTe provides similar conclusions as has been found for GaTe. The calculated data are given in Table S1 of Supporting Information.

Table 5. Calculated and experimental phonon frequencies (cm^{-1}) in tetragonal (*t*) phase of InTe. (R, IR - Raman and infrared active modes, S-silent modes.)

Mode	This work	[39]	Activity
E_g	22	-	R
A_{2g}	28	-	S
A_{2u}, TO	34	-	IR
A_{2u}, LO	47	-	IR
E_u, TO	38	-	IR
E_u, LO	48	-	IR
E_g	49	49	R
E_u, TO	69	-	IR
E_u, LO	88	-	IR
B_{1g}	73	86	R
A_{2g}	80	-	S
B_{2g}	87	-	R
B_{1u}	109	-	S
A_{1g}	129	126	R
E_g	141	139	R
A_{2u}, TO	146	-	IR
A_{2u}, LO	173	-	IR
E_u, TO	165	-	IR
E_u, LO	175	-	IR
B_{2g}	191	-	R

Table 5 lists the bulk frequencies calculated for the tetragonal phase of InTe. To the best of our knowledge, there is only one experimental work [39] by Nizametdinova, where the results of frequency measurements on indium telluride single crystals were reported. The author found and assigned four Raman values, which are in good agreement with our results. The calculated IR frequencies are susceptible to distinguishable LO-TO splitting, which can reach 30 cm^{-1}.

In Tables 6 and 7, we compare the vibrational frequencies of GaTe and InTe bulk 2H phases with corresponding monolayers' frequencies. In this case, the vibrational modes of bulk phases can be interpreted as arising from the splitting of monolayers' modes since the bulk UC is composed of two monolayers. In Tables 6 and 7 the symmetry of the original monolayer modes is given in the seventh column, while the split bulk modes are given in the first and fourth columns of the tables. In the bulk phases, there are two "interlayer" low-frequency modes (R: E_{2g} and S: B_{1g}) that are absent in monolayers. The calculated frequencies of the other modes in 3D and 2D systems are very close; the average deviation is about 3 cm^{-1}. However, as shown by Shenoy et al. [41], GaTe monolayers demonstrate peaks of higher intensity at frequencies higher than 300 cm^{-1} while the GaTe bulks show the most intense peaks at frequencies between 100 and 130 cm^{-1} in both the monoclinic and hexagonal cases. The Raman active optical modes have the following composition:

$$2A_{1g} + 2E_{1g} + 2E_{2g} \text{ (2H bulk)} \quad \text{and} \quad 2A_1' + 2E'' + E' \text{ (}h\alpha\text{-monolayer).} \qquad (3)$$

Although 6 different Raman frequencies can be detected in a bulk crystal, and only 5 in a monolayer, one of the 6 frequencies in the bulk spectrum is very low (10–15 cm^{-1}), and therefore can hardly be detected. As follows from our data in Tables 4, 6, and 8, Raman and IR bands in the range 140–160 cm^{-1}, which are absent in the GaTe hexagonal polymorphs,

should be observed in monoclinic bulk and its monolayer. This circumstance may help to distinguish the *rα hα* monolayers.

Table 6. Correspondence between the calculated vibrational modes of bulk (2H) phase and *hα* monolayer of GaTe. (R, IR - Raman and infrared active modes, S-silent modes.)

Bulk Mode	ν (cm^{-1})	Activity	Bulk Mode	ν (cm^{-1})	Activity	Monolayer Mode	ν (cm^{-1})	Activity
E_{1u}	0	–	E_{2g}	15	R	E'	0	–
A_{2u}	0	–	B_{1g}	40	S	A_2''	0	–
E_{2u}	38	S	E_{1g}	40	R	E''	42	R
B_{2u}	102	S	A_{1g}	112	R	A_1'	103	R
E_{2u}	174	S	E_{1g}	174	R	E''	178	R
E_{1u}, TO [a]	182	IR	E_{2g}	182	R	E'	184	IR/R
A_{2u}, TO [b]	205	IR	B_{1g}	210	S	A_2''	211	IR
B_{2u}	309	S	A_{1g}	309	R	A_1'	312	R

[a] E_{1u}, LO: 206 cm^{-1}.
[b] A_{2u}, LO: 209 cm^{-1}.

Table 7. Correspondence between the calculated vibrational modes of bulk (2H) phase and *hα* monolayer of hypothetical hexagonal InTe. (R, IR - Raman and infrared active modes, S-silent modes.)

Bulk Mode	ν (cm^{-1})	Activity	Bulk Mode	ν (cm^{-1})	Activity	Monolayer Mode	ν (cm^{-1})	Activity
E_{1u}	0	–	E_{2g}	12	R	E'	0	–
A_{2u}	0	–	B_{1g}	32	S	A_2''	0	–
E_{2u}	24	S	E_{1g}	26	R	E''	21	R
B_{2u}	87	S	A_{1g}	94	R	A_1'	87	R
E_{2u}	135	S	E_{1g}	135	R	E''	138	R
E_{1u}, TO*	141	IR	E_{2g}	141	R	E'	144	IR/R
A_{2u}, TO*	163	IR	B_{1g}	168	S	A_2''	169	IR
B_{2u}	216	S	A_{1g}	216	R	A_1'	217	R

[a] E_{1u}, LO: 165 cm^{-1}.
[b] A_{2u}, LO: 168 cm^{-1}.

Table 8. Calculated phonon frequencies (cm^{-1}) of hypothetical bulk 3R phases and *hβ* hexagonal monolayers of GaTe and InTe. (R, IR - Raman and infrared active modes, S-silent modes.)

Mode	GaTe Bulk	GaTe Monolayer	InTe Bulk	InTe Monolayer	Activity
E_u	0	0	0	0	–
A_{2u}	0	0	0	0	–
E_g	41	44	26	25	R
A_{1g}	108	102	94	87	R
E_g	173	180	135	140	R
E_u, TO	182	186	141	145	IR
E_u, LO	207		166		IR
A_{2u}, TO	201	209	163	168	IR
A_{2u}, LO	206		168		IR
A_{1g}	310	314	217	217	R

10.1002/ejic.202000634

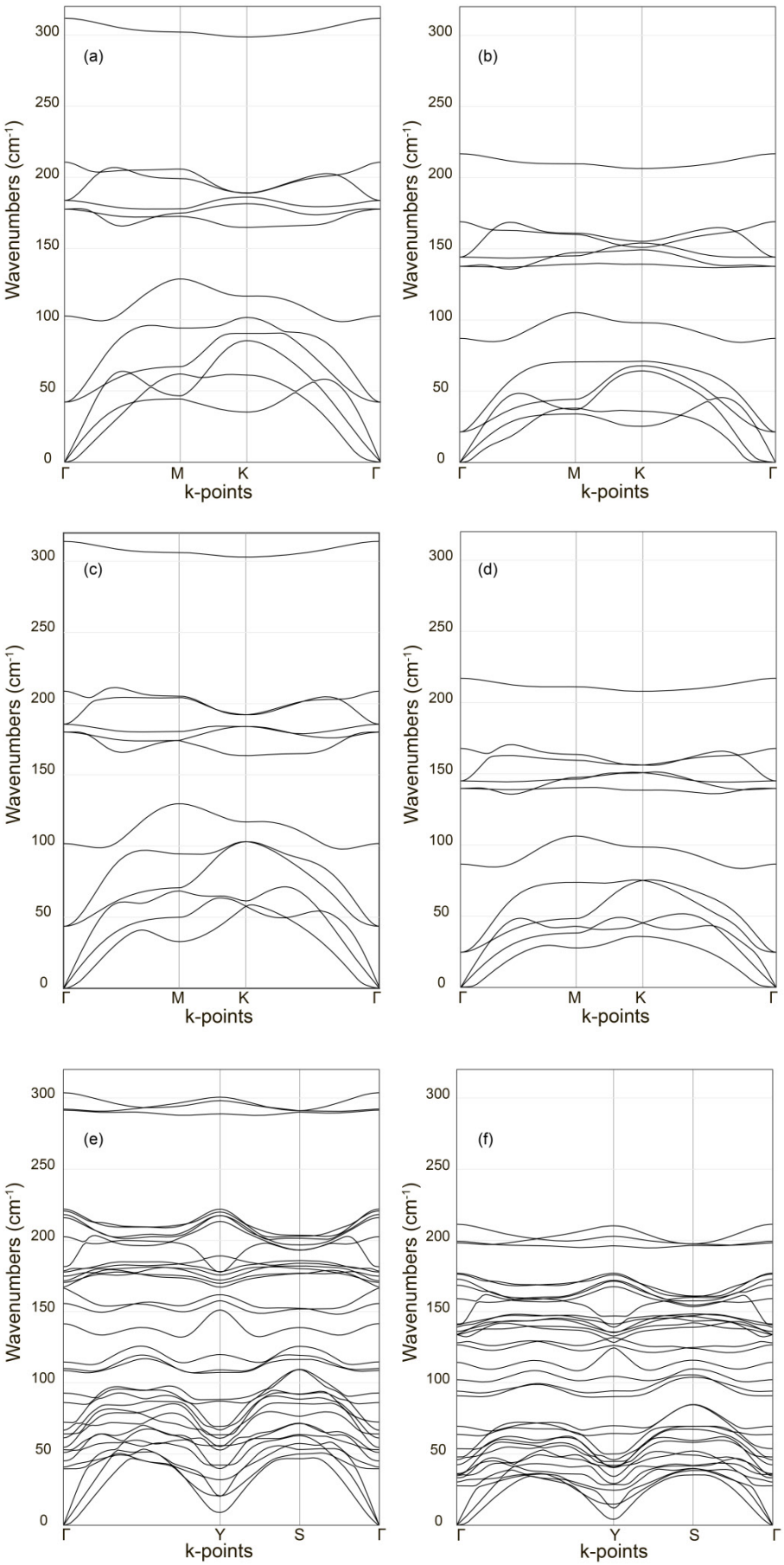

Figure 3. Phonon dispersion for monolayers. GaTe *hα* (a), InTe *hα* (b), GaTe *hβ* (c), InTe *hβ* (d), GaTe *rα* (e), InTe *rα* (f). See text for monolayer notation.

Table 8 includes our results for GaTe and InTe 3R rhombohedral phases and related *hβ* monolayers. As was pointed before, the properties of bulk 2H and 3R phases and their monolayers' properties are very similar. Collation of data given in Tables 6 and 7, on the one hand, and in Table 8, on the other hand, shows that the difference between the frequencies of the analogues modes does not exceed 5 cm^{-1}. However, Zólyomi et al. [51] pointed out that *hα* and *hβ* monolayers of InTe may be distinguished by comparing the number of Raman active phonon modes. Actually, in the case of 3R phase and *hβ* monolayer, the set of Raman active optical modes includes:

$$2E_g + 2A_{1g} \text{ (3R bulk and } h\beta\text{-monolayer)}. \quad (4)$$

Hence, the *hβ* monolayer possesses one twice-degenerated mode less than in the case of a *hα*-monolayer (see Eq. 3). Note also that the (isogonal) point group of the *hβ*-monolayer is D_{3d}, and the point group of the *hα*-monolayer is D_{3h}. The first structure has an inverse symmetry, but the second one does not.

Using the supercells mentioned in the Computational details section, we have simulated the phonon dispersion for all selected monolayers, which is plotted in Figure 3a–f. We found no imaginary modes, so all the considered monolayers should be the dynamically stable systems.

The hexagonal *hα* and *hβ* monolayers exhibit the same arrangement of the vibrational bands under the obvious condition that InTe has the lower frequencies due to the larger In atomic mass. Acoustic and low-frequency optical branches are separated from the middle-frequency branches by a prominent gap. Two separated A_1 branches lay above the first and second frequency bands. In the case of *rα* monolayer, the gap between the low and middle-frequency branches is not observed, and only three high-frequency branches are separated from the rest.

Different views exist in the literature on the magnitude of LO-TO splitting for monolayers. For example, Zólyomi et al. [51] supposed that the Coulomb nonanalytic contributions to the dynamical matrix could be ignored in monolayers. On the contrary, Shafique and Shin [54] found a stronger dipole-dipole interaction in InTe monolayers than in the corresponding bulk phases due to lower high-frequency dielectric constant of the monolayers. Taking into account the results of this study [54], we can expect that LO-TO splitting may be important for the upper E' and E_u modes in *hα* and *hβ* monolayers, accordingly. Nevertheless, due to our software's limitations, we did not calculate the LO-TO splitting in monolayers.

3.3. Thermodynamic properties and stability of bulk and monolayer GaTe and InTe

The phonon calculations at different k-points and summing their contributions over the BZ allow us to estimate the temperature dependences of the thermodynamic functions of the selected bulk and monolayer GaTe and InTe systems. The well-known statistical-thermodynamic equations (see, for example, Refs. [72,73]) have been used for this purpose.

In Figure 4, we compare the calculated and experimental [30,31] heat capacities and entropies of the most stable monoclinic and tetragonal phases of GaTe and InTe, accordingly. Complete thermodynamic data for bulk Ga and In tellurides were obtained in the early work of Kerimov et al. [29] and more recent studies by Tyurin and Gavrichev with co-authors [30,31] . The calibration results reported in these works evidenced that the error of heat capacity at constant pressure (C_p) did not exceed 0.25-0.30% at 50-300 K, while below 50 K, the deviations were somewhat larger. This means that the supposed experimental C_p error is about 0.1 J mol^{-1} K^{-1} below 300 K. Actually, the experimental error should be larger, since the

discrepancy between the old data [29] and the recent data [30,31] is significant and can reach 3 J mol^{-1} K^{-1} in the case of InTe heat capacity (the old C_p values [29] are noticeably lower than the more recent values [31]). It should be assumed that recent data [30,31] are more accurate; therefore, only they are presented in Figure 4.

For heat capacity, the noticeable discrepancy between the experimental C_p and calculated isochoric (at constant volume) heat capacity (C_v) appears after 200 K due to different equilibrium conditions with the environment used for calculated and measured quantity. It is known that C_p, becomes greater for solids [73] than C_v, at elevated temperatures T. The experimental determination of C_v would be possible if the precise temperature dependences of the volume thermal expansion coefficient and bulk modulus were known [73]. Instead of this, the authors of the work [31] proposed to estimate the C_p - C_v difference using the approximate Nernst-Lindemann equation [74]:

$$C_p - C_v = 0.00122\, C_p^2 T/T_m \quad (5)$$

where T_m is the melting temperature, and C_p, C_v – in J mol^{-1} K^{-1}. The melting points of GaTe and InTe phases under consideration are 1097 K [75] and 965 K [76], respectively. Following this approach, in Figure 4a, we plotted the experimental C_v converted from C_p [30,31] by the Nernst-Lindemann equation [74].

The discrepancy between the experimental and calculated C_v is still visible in Figure 4a at temperatures above 300 K, which is possibly due to anharmonic contributions. The harmonic heat capacity at constant volume must obey the Dulong-Petit limiting law at high temperatures, and calculated C_v values demonstrate this behavior, tending to 6R (R is the gas constant) with increasing temperature. In the case of entropy, the agreement between theoretical and measured values can be considered perfect (see Figure 4b).

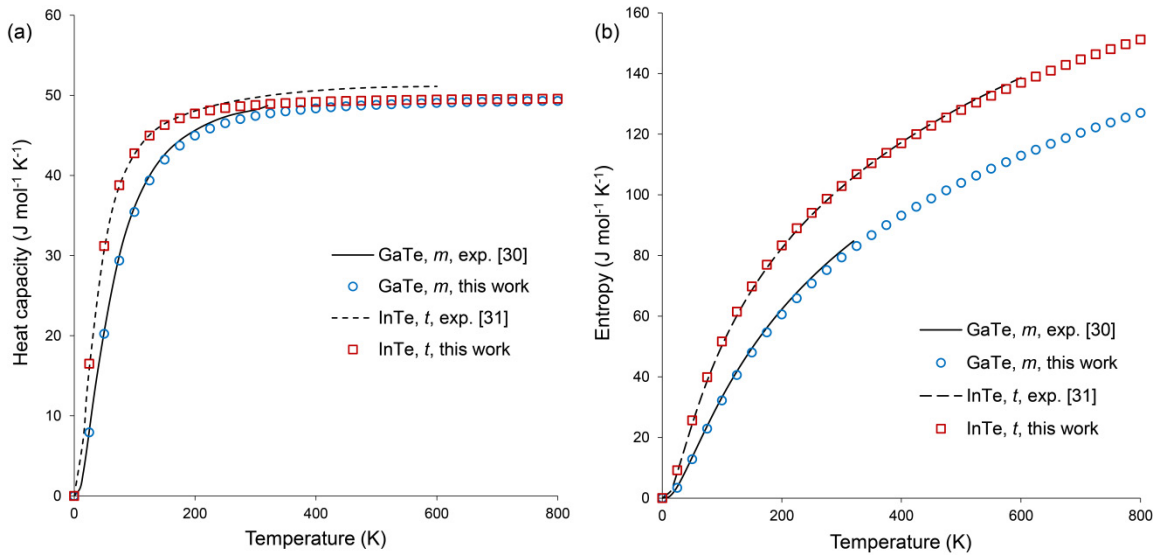

Figure 4. Temperature dependences of calculated and experimental isochoric heat capacity (a) and entropy (b) of the stable monoclinic (m) GaTe and tetragonal (t) InTe bulk phases. (All values are given per mole of formula units.)

The calculated thermodynamic functions of hexagonal GaTe are very close to those for monoclinic polymorph. For this reason, the obtained heat capacity and entropy of the hexagonal GaTe phase are not displayed in Figure 4 because they would not be distinguishable on the current scale. In contrast, the thermodynamic functions of tetragonal and hypothetical hexagonal InTe phases differ significantly (see Supporting Information, Figure S2). The estimated heat capacities of $h\alpha$, $h\beta$, and $r\alpha$ monolayers (shown in the

Supporting Information on Figure S3) at temperatures greater than 200 K practically coincide with the same functions of the hexagonal phases within the supposed computation accuracy (±0.1 J mol^{-1} K^{-1}). The deviation of the C_v of monolayers from that of 2H phases is given in Figure S4a. It can be seen that at low temperatures, the difference between the heat capacity of monolayers is more noticeable. The corresponding deviations in entropies are on the order of 1 J mol^{-1} K^{-1} (see Supporting Information, Figure S4b).

To verify the conclusions on the stability of bulk phases and monolayers based on the total energy calculations and to estimate the influence of temperature on this stability, the Helmholtz free energy has been calculated for the above-mentioned bulk phases and monolayers. Obviously, only the difference between the Helmholtz free energy of various states makes sense. For the sake of clarity, we have chosen the stable bulk phases as the reference systems. In Figure 5a, we show the Helmholtz free energies of formation (A_{form}) of GaTe and InTe hexagonal (2H) bulk phases with respect to monoclinic and tetragonal polymorphs, accordingly. It easy to see, that the temperature dependences of those thermodynamic functions are dissimilar: the A_{form}(GaTe, *h*) slowly increases remaining positive, while the A_{form}(InTe, *h*) increases sharply with a temperature rising. Thus, we can conclude that the stability of the hexagonal phase of GaTe depends on temperature quite weakly, but the hypothetical hexagonal phase of InTe becomes much more unstable relative to the tetragonal one at elevated temperatures. This fact makes improbable the synthesis of InTe hexagonal polymorph at normal or high temperatures.

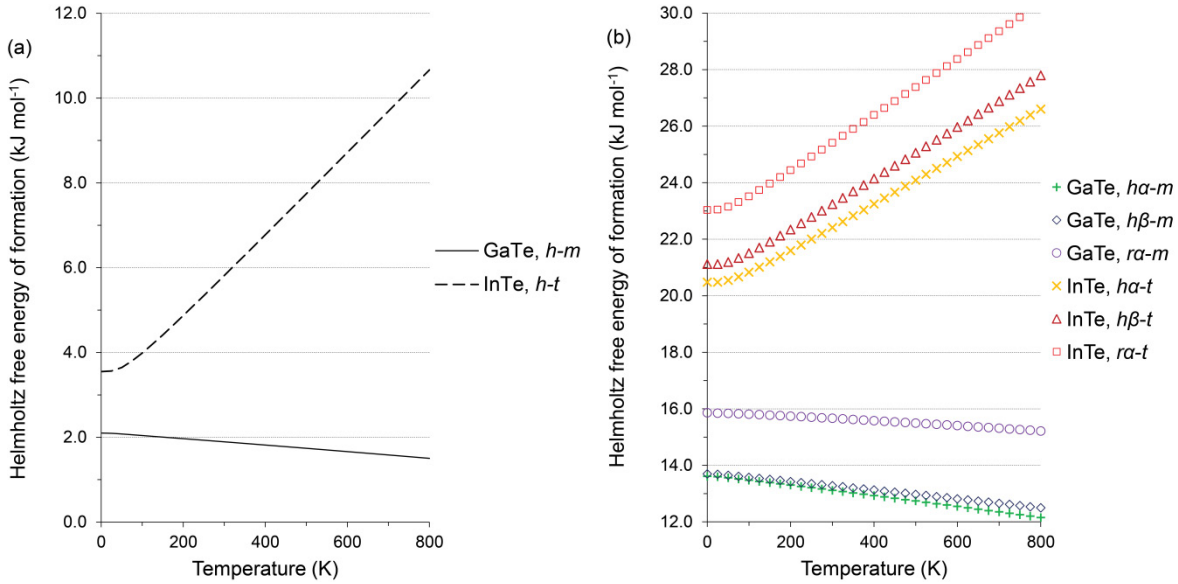

Figure 5. Calculated temperature dependence of Helmholtz free energy formation of hexagonal (*h*) bulks (a), as well as *hα*, *hβ*, and *rα* monolayers (b) from the stable monoclinic (*m*) GaTe and tetragonal (*t*) InTe bulk phases.

The formation free energy of monolayers is depicted in Figure 5b. The value of A_{form} is positive for all monolayers. The plots of $A_{\text{form}}(T)$ for three GaTe monolayers have a small and almost equal negative slope that is somewhat greater than the slope for hexagonal phase in Figure 5a. The formation energy of *hβ* monolayer almost coincides with that of *hα* monolayer in the entire temperature range, while the formation energy of *rα* monolayer is shifted upward by about 2 kJ mol^{-1}. The plots of $A_{\text{form}}(T)$ for three InTe monolayers have a large and positive slope similar to that in the bulk hexagonal phase (see Figure 5a). Again, the curve for the formation energy of *rα* monolayer lies above the curves for *hα* and *hβ* monolayers. Thereby, calculated monolayer thermodynamic functions confirm the

conclusions made based on the total energies that the rectangular monolayers are less stable than the hexagonal monolayers and the difference between the stability of *hα* and *hβ* monolayers is small. Simultaneously, the dependences displayed in Figure 5b demonstrate that a temperature increase somewhat facilitates the formation of a monolayers in the case of GaTe, but prevents it in the case of InTe.

Figures 5b and S5 (in Supporting Information) demonstrate that influence of the temperature on the relative difference between the Helmholtz free energies of monolayers with the same composition is weakly expressed. Only a slow increase in the difference between monolayer A_{form} can be recognized with a temperature rising, which is somewhat more intensive in the case of InTe monolayers (see Figure S5).

4. Conclusions

In this work, we performed a first-principles study on structural, vibrational, and thermodynamic properties of various bulk phases of gallium and indium tellurides, as well as their monolayer counterparts. The main goal of our modelling is to determine the most stable nanostructures which have a nonzero probability of being synthesized in the future. Moreover, the most stable monolayers can be considered as candidates for rolling up the nanotubes, whose properties should be the subject of our future research. The careful choice of the exchange-correlation functional, atomic basis sets, and dispersion corrections allow us to reproduce with good quality the experimental values of bulk phonon frequencies and the available temperature dependences of such thermodynamic functions as heat capacity and entropy.

First-principles modelling well reproduces the fact that the monoclinic and tetragonal phases are the ground states of GaTe and InTe bulk crystals, respectively. Comparative analysis of the thermodynamic stability of the metastable hexagonal modification of GaTe based on the Helmholtz free energy calculation shows that the stability of this polymorph weakly depends on temperature. In contrast, the hypothetical hexagonal phase of InTe becomes much more unstable relative to the tetragonal one at elevated temperatures. This circumstance leaves the possibility of synthesizing this phase at low temperatures only.

The calculation of the total energy of four possible monolayer structures MTe (M = Ga, In) indicates that their stability decreases in the following order: $h\alpha \geq h\beta > r\alpha >> r\beta$, where *hα* and *hβ* are the hexagonal monolayer polytypes, while *rα* and *rβ* are the centered rectangular structures originated from the low pressure GaTe monoclinic polymorphs and high pressure InSe polymorphs, accordingly. The formation of the hexagonal monolayers from the InTe tetragonal phase requires more energy (by about 7 kJ mol^{-1}) than the formation of monolayers of the same structure from the GaTe monoclinic phase. The most important conclusion in this work is that the rectangular monolayer is really less stable than the hexagonal monolayers, although the difference between total energies is rather small 2-3 kJ mol^{-1} for both GaTe and InTe.

Calculated Helmholtz free energy confirms that *hα* and *hβ* hexagonal monolayers possess close stability, but the rectangular monolayers *rα* are less stable than the hexagonal ones. Moreover, the free energy estimation allows us to find out the important role of the temperature: the temperature increase favors the formation of monolayers in the case of GaTe, but prevents it in InTe.

Finally, we can note that the analysis of the theoretical and experimental vibrational frequencies analysis provides the criteria for the distinction of different monolayer structures. Firstly, the Raman and IR bands, which were found in the range 140–160 cm^{-1} are absent in

the GaTe hexagonal polymorphs, but should be observed in monoclinic bulk and its monolayer. Secondary, our results confirm the conclusion of Zólyomi et al. [51] that *hα* and *hβ* monolayers may be distinguished by comparing the number of Raman active phonon modes.

Acknowledgments
The reported study was funded by the Russian Foundation for Basic Research within the framework of research project no. 20-03-00271 and accomplished using the computational facilities of the Resource Center "Computer Center of St. Petersburg State University".

Author information
Dr. A. V. Bandura, A. V. Kovalenko, Dr. D. D. Kuruch, Prof. Dr. R. A. Evarestov
Quantum Chemistry Department, Institute of Chemistry, Saint Petersburg State University, 7/9 Universitetskaya Naberezhnaya, St. Petersburg, 199034, Russian Federation
E-mail: r.evarestov@spbu.ru

Keywords: Density functional calculations, Monolayers, Phonon dispersion, Polymorphism, Thermodynamics.

References

[1] H. L. Zhuang, G. Hennig, Chem. Mater. **2013**, *25*, 3232-3238.
DOI: https://dx.doi.org/10.1021/cm401661x

[2] Z. Wang, M. Safdar, M. Mirza, K. Xu, Q. Wang, Y. Huang, F. Wang, X. Zhan, J. He, Nanoscale **2015**, *7*, 7252-7258.
DOI: https://dx.doi.org/10.1039/c4nr07313d

[3] P. Reshmi, A. Kunjomana, K. Chandrasekharan, M. Meena, C. Mahadevan, Int. J. Soft Comput. Eng. **2011**, *1*, 228-232.

[4] Y. Wang, K. Szökölová, M. Z. M. Nasir, Z. Sofer, M. Pumera, ChemCatChem **2019**, *11*, 2634-2642.
DOI: https://dx.doi.org/10.1002/cctc.201900449

[5] W. Huang, L. Gan, H. Li, Y. Ma, T. Zhai, CrystEngComm **2016**, *18*, 3968-3984.
DOI: https://dx.doi.org/10.1039/c5ce01986a

[6] R. A. Evarestov, Theoretical Modeling of Inorganic Nanostructures. Symmetry and ab initio Calculations of Nanolayers, Nanotubes and Nanowires, 2-nd ed., Springer, Berlin-Heidelberg, **2020**, Chapter 8.

[7] A. Harvey, C. Backes, Z. Gholamvand, D. Hanlon, D. McAteer, H. C. Nerl, E. McGuire, A. Seral-Ascaso, Q. M. Ramasse, N. McEvoy, S. Winters, N. C. Berner, D. McCloskey, J. F. Donegan, G. S. Duesberg, V. Nicolosi, J. N. Coleman, Chem. Mater. **2015**, *27*, 3483-3493.
DOI: https://doi.org/10.1021/acs.chemmater.5b00910

[8] W. Jie, J. Hao, Two-Dimensional Layered Gallium Selenide: Preparation, Properties, and Applications, in: Advanced 2D Materials (Eds.: A. Tiwari, M. Syväjärvi), Scrivener Publishing, Beverly, **2016**, pp. 1-36.
DOI: https://doi.org/10.1002/9781119242635.ch1

[9] D. J. Late , B. Liu, J. Luo, A. Yan, H. S. S. R. Matte, M. Grayson, C. N. R. Rao, V. P. Dravid, Adv. Mater. **2012**, *24*, 3549-3554.
DOI: https://doi.org/10.1002/adma.201201361

[10] M. Julien-Pouzol, S. Jaulmes, M. Guittard F. Alapini, Acta Crystallogr. B **1979**, *35*, 2848-2851.
DOI: https://doi.org/10.1107/S0567740879010803

[11] T. Karakostas, J. G. Antonopoulos, S. C. Kokkou, G. L. Bleris, N. A. Economou, phys. stat. sol. (a) **1980**, *59*, K17-K19.
DOI: https://doi.org/10.1002/pssa.2210590158

[12] M. K. Jacobsen, Y. Meng, R. S. Kumar, A. L. Cornelius, J. Phys. Chem. Solids **2013**, *74*, 723-728.
DOI: https://dx.doi.org/10.1016/j.jpcs.2013.01.011

[13] S. A. Semiletov, V. A. Vlasov, Sov. Phys. Crystallogr. **1964**, *8*, 704-708.

[14] N. N. Kolesnikov, E. B. Borisenko, D. N. Borisenko, A. V. Timonina, J. Cryst. Growth **2013**, *365*, 59-63.
DOI: https://dx.doi.org/10.1016/j.jcrysgro.2012.11.038

[15] M. P. Pardo, J. Flahaut, Sur une nouvelle forme de GaS, rhomboédrique 3R métastable. Formation et étude structural (Fr.), Mater. Res. Bull. **1987**, *22*, 323-329.
DOI: https://doi.org/10.1016/0025-5408(87)90048-1

[16] V. V. Karpov, A. V. Bandura, R. A. Evarestov, Phys. Solid State **2020**, *62*, 1017-1023.
DOI: https://doi.org/10.1134/S1063783420060116

[17] J. H. C. Hogg, H. H. Sutherland, Acta Cryst. B **1976**, *32*, 2689-2690.
DOI: https://doi.org/10.1107/S056774087600856X

[18] A. Kuhn, A. Bourdon, J. Rigoult, A. Rimsky, Phys. Rev. B **1982**, *25*, 4081-4088.
DOI: https://doi.org/10.1103/PhysRevB.25.4081

[19] K. Schubert, E. Dörre, M. Kluge, Z. Metallkd. **1955**, 46, 216-224.

[20] K. Cenzual, L. M. Gelato, M. Penzo, E. Parthé, Acta Crystallogr. B **1991**, *47*, 433-439.
DOI: https://doi.org/10.1107/S0108768191000903

[21] M. M. Nassary, Turk. J. Phys. **2006**, *30*, 95-102.
DOI: https://doi.org/10.3906/vet-1204-32

[22] J. L. Brebner, G. Fischer, E. Mooser, J. Phys. Chem. Solids **1962**, *23*, 1417-1421.
DOI: https://doi.org/10.1016/0022-3697(62)90194-4

[23] S. Pal, D. N. Bose, Solid State Commun. **1996**, *97*, 725-729.
DOI: https://doi.org/10.1016/0038-1098(95)00608-7

[24] U. Giorgianni, G. Mondio, P. Perillo, G. Saitta, G. Vermigho, Infrared and UV-visible spectra of layer semiconductors Gas, GaSe and GaTe, J. Phys. France **1977**, *38*, 1293-1299.
DOI: https://doi.org/10.1051/jphys:0197700380100129300

[25] U. Schwarz, K. Syassen, R. Kniep, J. Alloy. Compd. **1995**, *224*, 212-216.
DOI: https://doi.org/10.1016/0925-8388(95)01559-0

[26] T. K. Chattopadhyay, R. P. Santandrea, H. G. von Schnering, J. Phys. Chem. Solids **1985**, *46*, 351-356.
DOI: https://doi.org/10.1016/0022-3697(85)90178-7

[27] F. Birch, Phys. Rev. **1947**, *71*, 809-824.
DOI: https://doi.org/10.1103/PhysRev.71.809

[28] I. G. Kerimov, N. G. Aliev, M. M. Kurbanov, Fizika i Tekhnika Poluprovodnikov **1973**, *7*, 2366-2367.

[29] I. G. Kerimov, K. K. Mamedov, M. I. Mekhtiev, V. N. Kostryukov, Zhurnal Fizicheskoi Khimii **1971**, *45*, 1969-1972.

[30] A. V. Tyurin, K. S. Gavrichev, V. P. Zlomanov, N. N. Smirnova, Inorg. Mater. **2006**, *42*, 855-858.
DOI: https://doi.org/10.1134/S0020168506080097

[31] K. S. Gavrichev, L. N. Golushina, V. E. Gorbunov, G. A. Sharpataya, A. V. Khoroshilov, A. D. Izotov, 0. V. Ilyukhin, A. V. Tyurin, V. P. Zlomanov, V. M. Gurevich, Russ. J. Phys. Chem. A **2001**, *75*, Suppl. 1, S100-S104.

[32] S. Y. Back, H. Cho, Y.-K. Kim, S. Byeon, H. Jin, K. Koumoto, J.-S. Rhyee, AIP Advances **2018**, *8*, 115227.
DOI: https://doi.org/10.1063/1.5063274

[33] G. B. Abdullaev, L. K. Vodopyanov, K. R. Allakhverdiev, L. V. Golubev, S. S. Babaev, E. Y. Salaev, Solid State Commun. **1979**, *31*, 851-855.
DOI: https://doi.org/10.1016/0038-1098(79)90402-2

[34] J. C. Irwin, B. P. Clayman, D. G. Mead, Phys. Rev. B **1979**, *19*, 2099-2105.
DOI: https://doi.org/10.1103/PhysRevB.19.2099

[35] G. L. Belenkii, L.N. Alieva, R. Kh. Nani, E. Yu. Salaev, V. Ya. Shteinshraiber, Fizika Tverdogo Tela **1977**, *19*, 282-284.

[36] N. M. Gasanly, B. M. Dzhavadov, V.I. Tagirov, E. A. Vinogradov, phys. stat. sol. (b) **1980**, *100*, K53-K57.
DOI: https://doi.org/10.1002/pssb.2221000153

[37] A. Yamamoto, A. Syouji, T. Goto, E. Kulatov, K. Ohno, Y. Kawazoe, K. Uchida, N. Miura, Phys. Rev. B **2001**, *64*, 035210.
DOI: https://doi.org/10.1103/PhysRevB.64.035210.

[38] T. Wang, Q. Zhao, Y. Miao, F. Ma, Y. Xie, W. Jie, Crystals **2018**, *8*, 74.
DOI: https://doi.org/10.3390/cryst8020074

[39] M. A. Nizametdinova, phys. stat. sol. (b) **1980**, *97*, K9-K12.
DOI: https://doi.org/10.1002/pssb.2220970145

[40] E. G. Gillan, A. R. Barron, Chem. Mater. **1997**, *9*, 3037-3048.
DOI: https://doi.org/10.1021/cm9703886

[41] U. S. Shenoy, U. Gupta, D. S. Narang, D. J. Late, U. V. Waghmare, C.N.R. Rao, Chem. Phys. Lett. **2016**, *651*, 148-154.
DOI: https://dx.doi.org/10.1016/j.cplett.2016.03.045

[42] Q. Zhao, T. Wang, Y. Miao, F. Ma, Y. Xie, X. Ma, Y. Gu, J. Li, J. He, B. Chen, S. Xi, L. Xu, H. Zhen, Z. Yin, J. Li, J. Ren, W. Jie, Phys. Chem. Chem. Phys. **2016**, *18*, 18719-18726.
DOI: https://dx.doi.org/10.1039/c6cp01963c

[43] S. Huang, Y. Tatsumi, X. Ling, H. Guo, Z. Wang, G. Watson, A. A. Puretzky, D. B. Geohegan, J. Kong, J. Li, T. Yang, R. Saito, M. S. Dresselhaus, ACS Nano **2016**, 10, 8964-8972.
DOI: https://doi.org/10.1021/acsnano.6b05002

[44] J. Susoma, L. Karvonen, A. Säynätjoki, S. Mehravar, R. A. Norwood N. Peyghambarian, K. Kieu, H. Lipsanen, J. Riikonen, Appl. Phys. Lett. **2016**, *108*, 073103.
DOI: https://dx.doi.org/10.1063/1.4941998

[45] Y. Yu, M. Ran, S. Zhou, R. Wang, F. Zhou, H. Li, L. Gan, M. Zhu, T. Zhai, Adv. Funct. Mater. **2019**, *29*, 1901012.
DOI: https://dx.doi.org/10.1002/adfm.201901012

[46] C. J. Bae, J. McMahon, H. Detz, G. Strasser, J. Park, E. Einarsson, D. B. Eason, AlP Adv. **2017**, *7*, 035113.
DOI: https://doi.org/10.1063/1.4978776

[47] S. Lei, L. Ge, S. Najmaei, A. George, R. Kappera, J. Lou, M. Chhowalla, H. Yamaguchi, G. Gupta, R. Vajtai, A. D. Mohite, P. M. Ajayan, ACS Nano **2014**, *2*, 1263-1272.
DOI: https://doi.org/10.1021/nn405036u

[48] H. Shangguan, L. Han, T. Zhang, R. Quhe, Q. Wang, S. Li, P. Lu, J. Electronic Mater. **2019**, *48*, 5988-5994. DOI: https://doi.org/10.1007/s11664-019-07323-2

[49] S. S. Abed Al- Abbas, M. K. Muhsin, H. R. Jappor, Chem. Phys. Lett. **2018**, *713*, 46-51.
DOI: https://doi.org/10.1016/j.cplett.2018.10.020

[50] A. V. Kosobutsky, S. Yu. Sarkisov, Phys. Solid State **2018**, *60*, 1686-1690.
DOI: https://dx.doi.org/10.1134/S1063783418090172

[51] V. Zólyomi, N. D. Drummond, V. I. Fal'ko, Phys. Rev. B **2014**, *89*, 205416.
DOI: https://doi.org/10.1103/PhysRevB.89.205416

[52] J. Jalilian, M. Safari, Phys. Lett. A **2017**, *381*, 1313-1320.
DOI: https://dx.doi.org/10.1016/j.physleta.2017.01.024

[53] M.-S. Li, K.-X. Chen, D.-C. Mo, S.-S. Lyu, Phys. Chem. Chem. Phys. **2019**, *21*, 24695-24701.
DOI: https://doi.org/10.1039/C9CP04666F

[54] A. Shafique, Y.-H. Shin, Sci. Reports **2020**, *10*, 1093.
DOI: https://doi.org/10.1038/s41598-020-57644-0

[55] S. B. Touski, M. Ariapour, M. Hosseini, Physica E **2020**, *118*, 113875.
DOI: https://doi.org/10.1016/j.physe.2019.113875

[56] Z. Chen, X. Guo, J. Tang, F. Xiong, W. Li, Y. Chen, R. Ang, ACS Appl. Mater. Interfaces **2019**, *11*, 26093-26099.
DOI: https://doi.org/10.1021/acsami.9b07222

[57] Z. Chen, X. Guo, F. Zhang, Q. Shi, M. Tang, R. Ang, J. Mater. Chem. A **2020**, *8*, 16790-16813.
DOI: https://doi.org/10.1039/d0ta05458e

[58] Zhiyu Chen, Jing Tang, Xuming Guo, Fujie Zhang, Mingjing Tang, Fen Xiong, Yue Chen, and Ran Ang, Appl. Phys. Lett. **2020**, *116*, 193902.
DOI: https://doi.org/10.1063/5.0006739

[59] T. Ayadi, L. Debbichi, M. Said, S. Lebègue, J. Chem. Phys. **2017**, *147*, 114701.
DOI: https://doi.org/10.1063/1.4997233

[60] J. P. Perdew, M. Ernzerhof, K. Burke, J. Chem. Phys. **1996**, *105*, 9982-9985.
DOI: https://doi.org/10.1063/1.472933.

[61] A. Kuzmin, A. Kalinko, R. A. Evarestov, Cent. Eur. J. Phys. **2011**, *9*, 502-509.
DOI: https://doi.org/10.2478/s11534-010-0091-z

[62] Y. Zhao, D. G. Truhlar, Theor. Chem. Acc. **2008**, *120*, 215-241.
DOI: https://doi.org/10.1007/s00214-007-0310-x

[60] R. Dovesi, A. Erba, R. Orlando, C. M. Zicovich-Wilson, B. Civalleri, L. Maschio, M. Rerat, S. Casassa, J. Baima, S. Salustro, B. Kirtman, WIREs Comput. Mol. Sci. **2018**, *8*, e1360.
DOI: https://doi.org/10.1002/wcms.1360

[64] R. Dovesi, V. R. Saunders, C. Roetti, R. Orlando, C. M. Zicovich-Wilson, F. Pascale, B. Civalleri, K. Doll, N. M. Harrison, I. J. Bush, Ph. D'Arco, M. Llunel, M. Causà, Y. Noël, L. Maschio, A. Erba, M. Rérat, S. Casassa, CRYSTAL17 User's Manual, University of Turin, Torino, Italy, **2017**. (Can be found under https://www.crystal.unito.it/index.php)

[65] D. Vilela Oliveira, M. F. Peintinger, J. Laun, T. Bredow, J. Comput. Chem. **2019**, *40*, 2364-2376
DOI: https://doi.org/10.1002/jcc.26013

[66] J. Heyd, J. E. Peralta, G. E. Scuseria, R. L. Martin, J. Chem. Phys. **2005**, *123*, 174101.
DOI: https://doi.org/10.1063/1.2085170

[67] H. J. Monkhorst, J. D. Pack, Phys. Rev. B **1976**, *13*, 5188-5192.
DOI: https://doi.org/10.1103/PhysRevB.13.5188

[68] S. Grimme, J. Antony, S. Ehrlich, H. Krieg, J. Chem. Phys. **2010**, *132*, 154104.
DOI: https://doi.org/10.1063/1.3382344

[69] A. Erba, A. Mahmoud, D. Belmonte, R. Dovesi, J. Chem. Phys. **2014**, *140*, 124703.
DOI: https://dx.doi.org/10.1063/1.4869144

[70] F. Pascale, C. M. Zicovich-Wilson, F. López-Gejo, B. Civalleri, R. Orlando, R. Dovesi, J. Comput. Chem. **2004**, *25*, 888-897.
DOI: https://dx.doi.org/10.1002/jcc.20019

[71] C. M. Zicovich-Wilson, F. Pascale, C. Roetti, V. R. Saunders, R. Orlando, R. Dovesi, J. Comput. Chem. **2004**, *25*, 1873-1881.
DOI: https://dx.doi.org/10.1002/jcc.20120

[72] D. C. Wallace, Thermodynamics of Crystals, Dover, New York, **1998**.

[73] F. Reif, Fundamentals of Statistical and Thermal Physics, Waveland Press, Long Grove, **2009**, p. 168

[74] W. Nernst, F. A. Lindemann, Z. Elektrochem **1911**, *17*, 817-827.

[75] F. Alapini, J. Flahaut, M. Guittard, S. Jaulmes, M. J. Julien-Pouzol, Solid State Chem. **1979**, *28*, 309-319.
DOI: https://doi.org/10.1016/0022-4596(79)90082-3

[76] K. C. Mills, Thermodynamic Data for Inorganic Sulphides, Selenides and Tellurides. Butterworth, London, **1974**.